Original Article
Bioluminescence imaging of therapy response does not correlate with FDG-PET response in a mouse model of Burkitt lymphoma

Marijke De Saint-Hubert[1], Ellen Devos[2], Abdelilah Ibrahimi[3], Zeger Debyser[3], Luc Mortelmans[2], Felix M Mottaghy[1,2,4]

[1]Department of Nuclear Medicine, Maastricht University Medical Centre, Maastricht, The Netherlands; [2]Department of Nuclear Medicine, Katholieke Universiteit Leuven, Leuven, Belgium; [3]Laboratory for Molecular Virology and Gene Therapy, Katholieke Universiteit Leuven, Leuven, Belgium; [4]Klinik für Nuklearmedizin, UKA, RWTH Aachen, Germany

Abstract: Since the development and evaluation of novel anti-cancer therapies require molecular insight in the disease state, both FDG-PET and BLI imaging were evaluated in a Burkitt B-cell lymphoma xenograft model treated with cyclophosphamide or temsirolimus. Daudi xenograft mice were treated with either cyclophosphamide or temsirolimus and imaged with BLI and FDG-PET on d0 (before treatment), d2, d4, d7, d9 and d14 following the start of therapy. Besides tumor volume changes, therapy response was assessed with immunohistochemical analysis (apoptosis). BLI revealed a flare following both therapeutics that was significantly higher when compared to control tumors. FDG-PET decreased immediately, long before the tumor reduced in size. Late after therapy, BLI signal intensities decreased significantly compared to baseline subsequent to tumor size reduction while apoptosis was immediately induced following both treatment regimen. Unlike FDG, BLI was not able to reflect reduced levels of viable cells and was not able to predict tumor size response and apoptosis response.

Keywords: Bioluminescence imaging, therapy response, FDG-PET

Introduction

For the development and evaluation of novel anti-cancer therapies it is crucial to monitoring tumor growth in research models. The traditional techniques to follow up tumor growth involve monitoring life span of animals or measuring tumor size with calipers, however these fail to capture minimal disease states. More detailed histological and molecular analysis of tumors may elucidate more information but necessitate animal sacrifice and therefore don't allow serial observations of response to therapy in the same animal over time. To overcome these limitations non-invasive imaging modalities allow to follow-up tumor response over time. Imaging of tumor size with computed tomography (CT) or magnetic resonance imaging (MRI) is limited because information on molecular response is minimal and tumor size reduction regularly occurs late after therapy. Positron

emission tomography (PET) using the glucose analogue 2-[18F]fluoro-2-deoxyglucose (FDG) allows to assess metabolic changes following effective treatment. In clinical oncology FDG-PET is an established imaging technique for cancer diagnosis and also demonstrates to be highly predictive for progression free survival and overall survival in several types of cancer patients [1-4]. This imaging modality has been adapted for small animals allowing to monitor therapy in animal models with microPET systems using FDG. Unfortunately, the specificity of FDG is limited, mainly because this tracer may as well accumulate in inflammatory cells, but also because certain therapies may alter glucose metabolism without tumor remission [5, 6]. Therefore FDG-PET can lead to an underestimation of therapy effects.

Recently, bioluminescence imaging (BLI) has been applied in a pre-clinical setting. Although it

is not applicable in a clinical setting it is an exceptionally sensitive technique with a superior signal-to-noise ratio that is easy to perform with limited costs. This imaging technique is based on luciferase enzymes that catalyze light production using small substrate molecules, luciferins [7-10]. Luciferase can be expressed constitutively in tumor cells to track survival and cell growth of these cells *in vivo* but is also useful to assess tumor mass and remaining tumor burden after therapy [11, 12]. To accurately quantify tumor cell number, the intensity of the BLI light signal should directly be related to the amount of viable cells. Since the penetration of photons can be influenced by tumor size, shape and vasculature the BLI signal can differ between tumors. Additionally, tumor cells should contain the same amounts of luciferase enzyme and amounts should be stable over time. This equilibrium can be influenced by changes in the inserted reporter gene DNA, expression of the reporter gene and luciferase protein degradation [13, 14]. Moreover, the enzymatic reaction is decisive and may critically vary because of the bioavailability and concentration of the products. Not only oxygen and ATP levels but also the luciferin biodistribution, vasculature and perfusion or membrane permeability and integrity may differ between certain biological conditions. M. Keyaerts et al. studied several biological factors affecting BLI quantification and were the first to show that changes in plasma protein concentrations significantly influenced BLI quantification [15].

These observations may be critical in the evaluation of therapy response since chemotherapeutic drugs can significantly influence biological factors and equilibriums. Indeed, some groups describe alterations in luciferase expression levels following chemotherapy and radiotherapy [14, 16, 17]. Despite these observations, several researchers elaborate BLI to measure changes in viable tumor cell fractions following anti-cancer therapy and do not consider therapy-associated changes [11, 12, 18].

In the current study we describe BLI response early after treatment of Burkitt B-cell lymphoma xenografts and correlate these results to sequential FDG-PET scans, measurements of tumor size and patho-physiological tumor responses as measured with immunohistochemistry (IHC). We examined response to cyclophosphamide, a standard chemotherapeutic that

induces cell death in rapidly growing cells, and also monitored the molecular mammalian target of rapamycin (mTOR) inhibitor, temsirolimus, which specifically induces cell cycle arrest of tumor cells.

Materials and methods

Cell line

The human B-lymphoblast cell line Daudi was derived from a Burkitt lymphoma [5]. Cells were cultured in DMEM medium without pyruvate and supplemented with 10 % fetal bovine serum (FBS), 1 % penicillin/streptomycin (P/S), 1 % L-glutamine, 1 % HEPES and 1 % sodium pyruvate. The cells were cultured in flasks in a humidified 5 % CO_2 atmosphere at 37 °C.

Daudi cells (Burkitt B-cell lymphoma) were transduced with a lentiviral vector (*pSFFV-BSdR-T2A-Fluc*) expressing both blasticidin selection marker and firefly luciferase bioluminescent reporter gene. The pCH-SFFV- BsdR-P2A-Fluc was constructed using standard cloning techniques. Briefly, the blasticidin antibiotic gene was amplified by PCR using AAATCTA-GAATGGCCAAGCCTTTGTCTCAAGAA as a sense primer and AAACTCGAGGCCCTCCCACACATAAC-CAGAGGG as anti-sense primer. The PCR product was digested with *XbaI* and *XhoI* and cloned downstream of the spleen focus forming virus (SFFV) promoter. Lentiviral vector was produced and concentrated as described by Ibrahimi et al. [19]. For transduction experiments cells were seeded in 24-well plate, 2.5×10^5 cells per well. The next day, the cells were transduced for 24 hours with vector preparations serially diluted in Daudi cells medium (as described above). The transduced cells were then grown in blasticidin-containing medium (2 μg/ml) for 4 days.

Animal model

Severe combined immune deficient (SCID)-mice (C.B-17/Icr *scid/scid)* were bred under germ-free conditions. Mice (6 to 8 weeks old) were inoculated with 5×10^6 LV-stably transduced Daudi cells in both shoulders. Developing tumors were monitored with BLI starting on week 0 (day of inoculation) and measured every week until week 7. As soon as the tumor was visually perceptible caliper measurements were performed. When the developing tumors had reached a diameter between 10 and 15 mm

mice were subjected to treatment.

Treatment regimen

Treatment was performed with a single dose of cyclophosphamide 125 mg/kg intraperitoneally (i.p.) (Endoxan, Baxter) on day 0 (d0). The mTOR inhibition was performed with temsirolimus 50 mg/kg i.p., which was provided by Wyeth (CCI-779, Torisel, Wyeth).

Caliper measurements

To assess tumor volume and track changes in tumor size we measured the tumor dimensions (n=9 for cyclophosphamide, n=10 for temsirolimus and n=10 for controls) using a caliper on d0 (before treatment), d2, d4, d7, d9, d14 following start of therapy (no treatment for controls). Tumor volumes (Vol_{calip}) were calculated using the equation $Vol_{calip} = (\pi/6) \times a \times b \times c \times 10^{-3}$ where a, b and c represent the three orthogonal axes of the tumors in millimeters.

In vivo bioluminescence imaging

BLI was performed on d0 (before treatment), d2, d4, d7, d9, d14 following start of therapy (no treatment for controls). The mice (n=5 per group) were anesthetized and imaged in an IVIS 100 system (Xenogen, Almeda, CA) as described previously [20]. The mice were i.p. injected with D-luciferin (126 mg/kg; Xenogen, Teralfene, Belgium) dissolved in phosphate buffered saline (PBS) (15 mg/l). Subsequently four to five mice were positioned in prone position in the IVIS system and frames were acquired with a field of view of 25 cm. Consecutive scans with acquisition times ranging from 1 to 60 seconds (s) were performed until the maximal signal was reached.

The quantification of BLI data was performed with Living Image software (version 2.50.1) (Xenogen, Almeda, CA). This program measures photon flux (p/s) from an oval shaped (2 cm width and 4 cm height) region of interest (ROI) on the tumor resulting in total 2D photon flux.

Small animal PET scanning

FDG-PET was performed on d0 (before treatment), d2, d4, d7, d9, d14 following start of cyclophosphamide (n=4) and temsirolimus therapy (n=5). A group of non-treated control animals (n=4) was followed up with FDG-PET on d0 (before treatment), d2, d6, d9 and d13. Small animal PET scanning was performed using a dedicated small animal PET (FOCUS 220 microPET; Concorde-CTI Siemens, Knoxville Tenessee, USA). Mice were fasted overnight and immediately before injection sedated by gas anesthesia with isoflurane, and body weight, tumor dimensions (caliper) and glycemia (in case of FDG) were determined. Then 8-11 MBq FDG was injected via a tail vein. Sixty minutes post-injection, PET imaging was performed (10 minutes/frame), on a single bed position with the tumor in the center of the view.

For PET tumor tracer uptake was measured with in-house software (IDL viewer) as previously described [21, 22]. Tracer uptake was defined as standardized uptake value (SUV) which is calculated by the equation: SUV = measured activity concentration in the tumor (Bq/g) x body weight (g) / injected activity (Bq). To correct for differences in administered dose (paravenous injections became more frequent after several injections), all SUVs were normalized by dividing SUV of the tumor by the corresponding SUV_{mean} of a standard region in the liver.

Statistical analysis

Within each animal changes in SUV, BLI signal or Vol_{calip} were calculated by the following formula: % SUV change = $(SUV_x-SUV_0)/SUV_0 \times 100$ % with SUV_x being the FDG-uptake at day x.

The statistical analysis was performed using GraphPad PRISM 5.04. In each treatment group mean % changes and standard error of the mean (SEM) were calculated and graphically expressed. For multiple comparisons, such as evaluation of mean changes over time, we performed one-way analysis of variances (ANOVA) and Bonferroni's multiple comparisons. In order to detect significant differences between parameters on different time points we performed two-way ANOVA and Bonferroni's multiple comparisons. A p-value <0.05 was defined as statistically significant.

Immunohistochemistry

On each time point following therapy paraffin embedded sections were stained with haematoxylin and eosin (H&E) and terminal deoxynucleotidyl transferase biotin-dUTP nick end label-

ing (TUNEL) to assess the number of dying cells (n=2 per time point).

TUNEL positive cells were counted in 10 HPF and expressed as positive cells/HPF.

Ethical committee

All animals were treated in concordance with institutional guidelines and experiments were approved by the local ethical committee for animal experiments.

Results

Bioluminescence imaging to measure response

BLI was performed in non-treated mice and in cyclophosphamide and temsirolimus treated mice (**Figure 1**). In control mice the signal increased over time and accordingly the tumor increased in size (see **Figure 2**). Following cyclophosphamide therapy we observed a significantly increased BLI signal on d4 compared to d0 (+199 %, see **Figure 1**) which was significantly higher than control values measured at that time point (p<0.005). It was only from day 14 that a significant reduction in BLI signal was measured (-80 %).

In **Figure 3** BLI is shown for a cyclophosphamide treated animal which clearly demonstrating increased BLI signal on day 2 and day 4. In this particular animal the BLI signal decreased from day 9 following therapy with almost complete disappearance of the signal on d14.

Also for temsirolimus animals the BLI signal increased 4 days after temsirolimus compared to d0 (+119 %, see **Figure 1**). Although the increased signal was less pronounced than the one obtained from cyclophosphamide treated mice, it was significantly higher than in control mice at that time point (p<0.05). From day 9 a
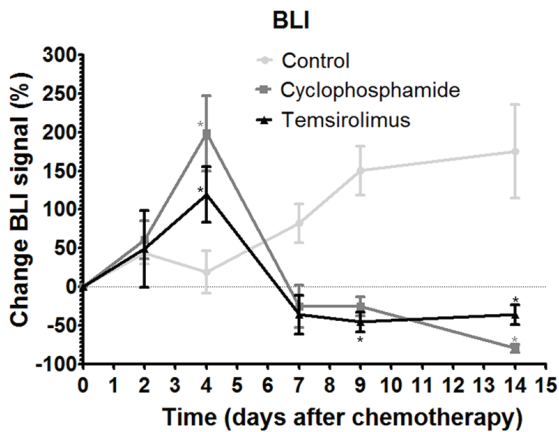

Figure 1. BLI response in control mice (●) (n=5), cyclophosphamide (■) (n=5) and temsirolimus (▲) (n=5) treated mice on d2, d4, d7, d9 and d14. The data are expressed as % change in mean BLI signal ±SEM compared to d0. *p-value <0.01 as compared to d0 measured with unpaired student's t-test.
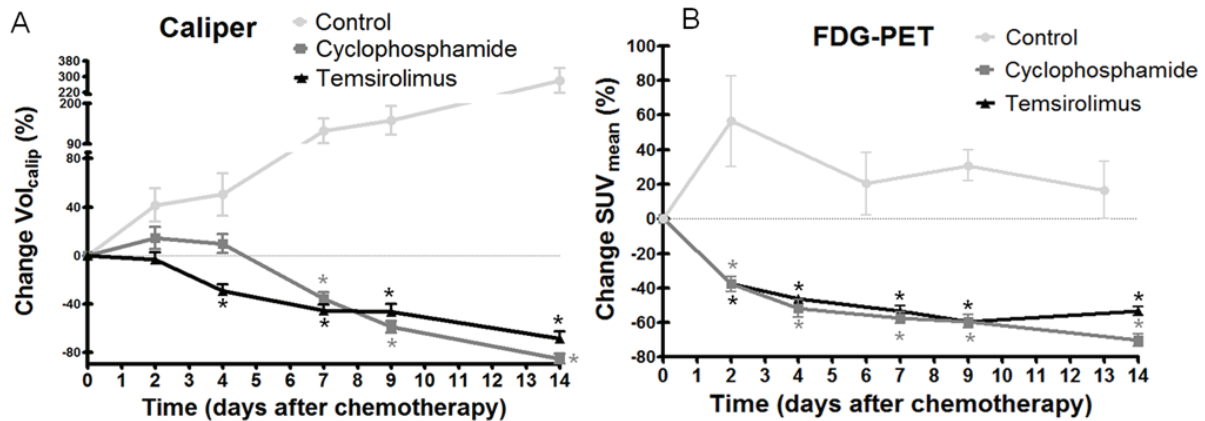

Figure 2. Changes in Vol$_{calip}$ (tumor volume measured by caliper) (A) (n≥9) and changes in FDG uptake as measured with SUV$_{mean}$ (B) (n≥4) during follow-up of control mice (●), cyclophosphamide treated mice (■) and temsirolimus treated mice (▲). The data presented as mean percentage changes in Vol$_{calip}$ and SUV$_{mean}$ ±SEM and measured on d0, d2, d4, d7, d9 and d14. *p-value <0.01 as compared to d0 with unpaired student's t-test.
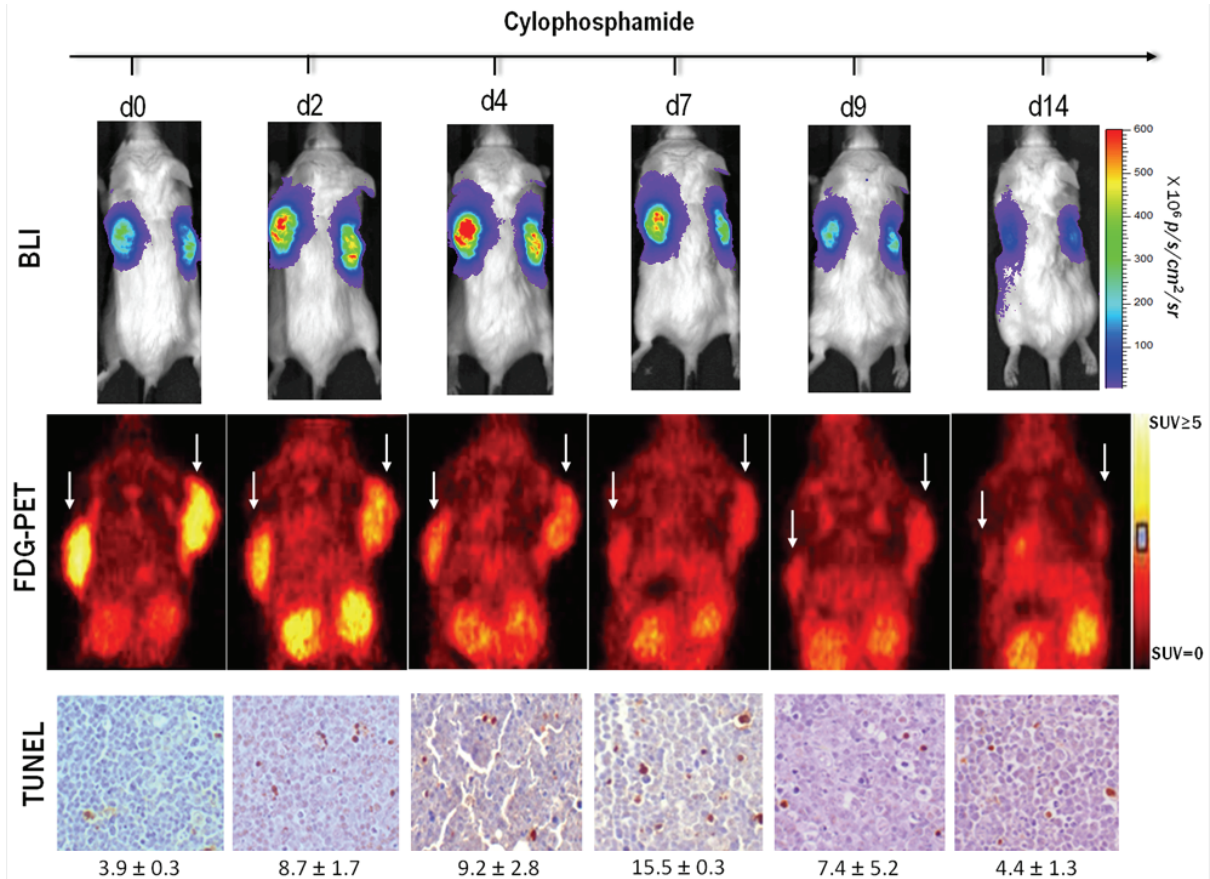
Figure 3. Example of cyclophosphamide treated mice, followed up with BLI and FDG-PET on d0, d2, d4, d7, d9 and d14. Transversal views are scaled as specified by the BLI color bar (0-600x10^6 p/s/cm^2/sr) and by the SUV color bar (SUV between 0-5). Corresponding TUNEL staining and TUNEL measures (number of positive cells/HPF) demonstrate early induction of apoptosis which was most pronounced 7 days after therapy.

significant reduction of the BLI signal (-41%) could be measured. In **Figure 4**, BLI shows increased signal between day 2 and day 7 while BLI decreased on day 9 following temsirolimus treatment of this animal.

Tumor volume measurement by caliper

Tumor volume in the control group showed a persistent increase during follow-up and mean Vol$_{calip}$ was increased with 280 ± 63% on d14 (**Figure 2A**). Early after cyclophosphamide treatment the tumor volume showed a tendency to increase in size (non-significant increase in Vol$_{calip}$ on d2 and d4) (**Figure 2A**). A significant reduction in Vol$_{calip}$ was seen from d7 (-33±7%) with a further decrease and an almost complete disappearance of the tumors on d14 (**Figure 2A**).

Caliper measurements in temsirolimus treated mice revealed a significant reduction in Vol$_{calip}$ on d4 (-29±9%) with a further decrease until d7 (-48±7%). Between d7 and d14 no significant size reduction was measured and in all treated mice tumor tissue remained detectable on d14 (**Figure 2A**).

FDG-PET to measure response

As shown in **Figure 2B** FDG uptake decreased immediately after cyclophosphamide administration compared to baseline (-38 % on d2 and -52 % on d4). Further decrease in SUV$_{mean}$ was measured and minimal on d14 following cyclophosphamide. **Figure 3** also demonstrates a fast reduction in FDG uptake while the metabolic tumor volumes reduce from day 7 after initiation of the therapy. On day 14 almost no
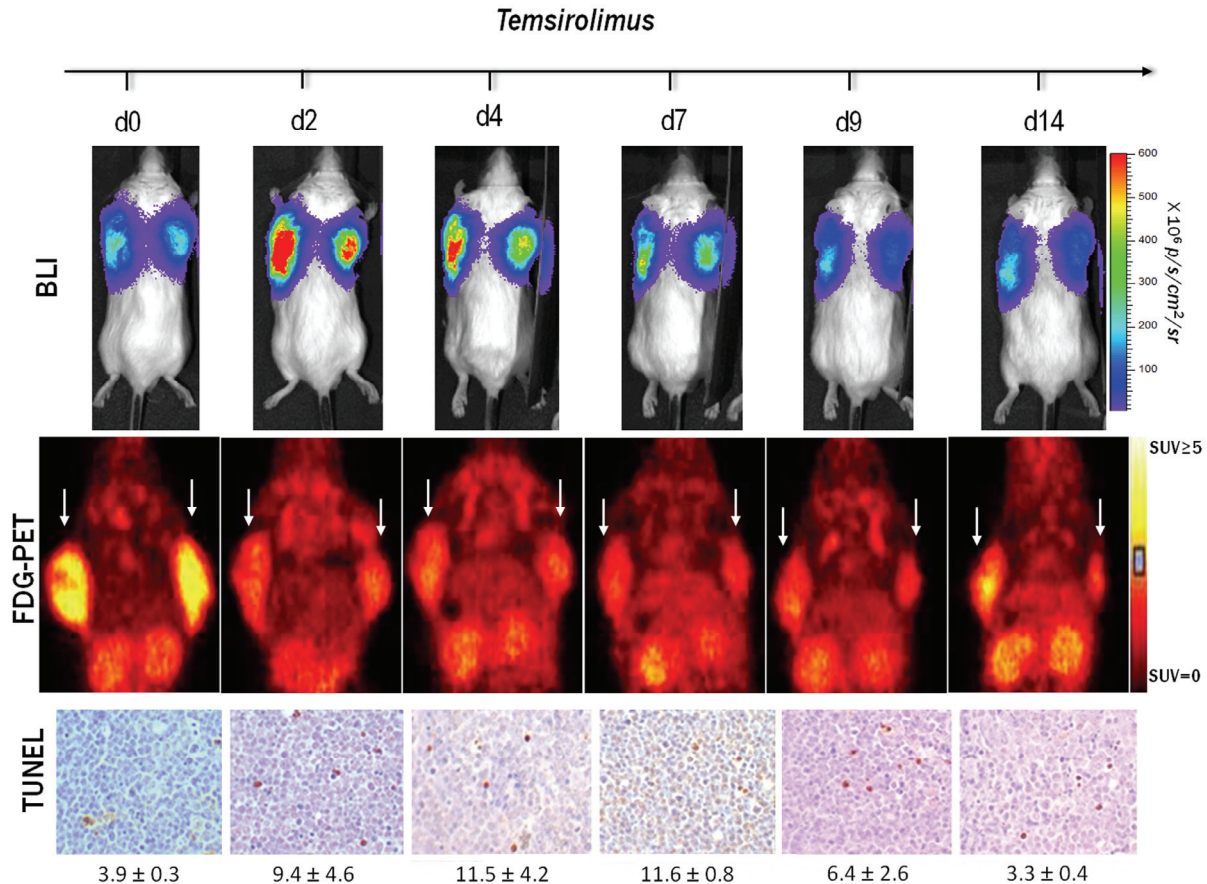
Figure 4. Example of temsirolimus treated mice, followed up with BLI and FDG-PET on d0, d2, d4, d7, d9 and d14. Transversal views are scaled as specified by the BLI color bar (0-600x10⁶ p/s/cm²/sr) and by the SUV color bar (SUV between 0-5). Corresponding TUNEL staining and TUNEL measures (number of positive cells/HPF) demonstrate induction of apoptosis on d2 until d9 following therapy.

FDG uptake was visible corresponding to almost complete disappearance of the tumor.

Also following temsirolimus an immediate reduction in FDG uptake was measured (-38% on d2 and -46% on d4 respectively) (**Figure 2B**). FDG uptake decreased further on d4 and d7 and reached a minimum on d9 (-59%) after which it stabilized (-53% on d14). **Figure 4** also depicts a fast reduction in FDG uptake following temsirolimus treatment while on day 14 the FDG uptake showed tendency to expand in this mouse.

Immunohistochemical analysis

Untreated tumors revealed only few TUNEL positive cells (3.9 ± 0.3/HPF) indicating a low level of spontaneous apoptosis in these mice. Upon cyclophosphamide treatment we observed a direct induction of cell death with TUNEL which was most pronounced 7 days after induction of the treatment (**Figure 3**). Temsirolimus treatment induced apoptosis on days 2 until day 9 (**Figure 4**). Compared to cyclophosphamide the induction of apoptosis was less pronounced for temsirolimus treatment.

Discussion

For the development and evaluation of novel anti-cancer therapies, solely tumor growth measurements often miss initial molecular tumor responses. Therefore molecular imaging of tumor response with FDG-PET has advanced into experimental study designs allowing to follow up therapeutic effects in dedicated tumor models. Nevertheless influx of inflammatory

cells can lead to underestimation of the therapeutic effects and allows only an indirect measurement of tumor viability. In this perspective the visualization of the number of viable tumor cells with BLI might allow an accurate, highly sensitive and easy technique to monitor therapeutic effects in preclinical animal models. Nevertheless BLI is a 2D imaging technique that is surface-weighted while FDG-PET measures metabolism in three dimensions. In the current study we evaluated BLI and compared results with FDG-PET and changes in tumor size. We chose to evaluate two types of treatment agents; cyclophosphamide, a standard chemotherapeutic, and temsirolimus, inducing mainly cell cycle arrest.

BLI analysis revealed largely augmented BLI signal intensities early after treatment which were considerably higher when compared to non-treated animals scanned on this time point. This effect seemed to be higher for cyclophosphamide compared to temsirolimus therapy. Surprisingly only few studies reported an increased BLI signal early after therapy which were suggested to be due to metabolic changes induced by the therapy such as changes in membrane permeability, ATP elevation due to stress response or apoptosis [19], degradation of the membrane integrity or transient changes in transcription [14]. The induction of apoptosis was more pronounced for cyclophoshpamide when compared to temsirolimus which may in part explain the higher BLI signal. Additionally cyclophoshamide is described to induce DNA repair early after therapy which also induces higher metabolic activity of cells [23]. Besides metabolic changes following therapy, the transcription of the promoter may be altered following toxic treatment. This was already described for the cytomegalovirus (CMV) promoter demonstrating BLI increase up to 3 times control values following cyclophosphamide therapy [14]. No such activation of the spleen focused forming virus (SFFV), used in the current study, has yet been described.

In a recent publication by M Keyaerts et al., the effect of protein concentrations has been demonstrated to have vast influence on BLI signal. In this regards, toxic therapies such as doxorubicin can induce hypoalbuminemia resulting in an increased BLI signal [15]. Although hypoalbuminemia has not been described for cyclophosphamide and temsirolimus, these toxic agents can influence plasma protein concentrations

and result in altered substrate binding leading to an increased BLI signal.

Overall, several processes may explain the increased BLI signal and most likely a combination resulted in the increased BLI levels. The specific assessment of the processes involved in this interplay was beyond the scope of this project and needs extensive in vitro and in vivo research. Unfortunately these results suggest that metabolic or molecular changes following therapy, not necessarily correlated to viability, can influence the BLI signal early after therapy which should be considered when used for response assessment.

Also on later time points, BLI failed to depict a decreased amount of viable cells earlier than tumor shrinkage. The BLI signal decreased significantly when tumor volumes were largely reduced for temsirolimus on day 9 (-47 ± 7% Vol_{calip}) and for cyclophosphamide on day 14 (-85 ± 4% Vol_{calip}). As a result BLI was not able to depict a reduced amount of viable cells while an undoubted reduction in the amount of viable cells was measured by caliper (Vol_{calip}) on day 4 for temsirolimus and day 7 for cyclophosphamide. This can be explained by the fact that the BLI flare was not restricted to the early time points following therapy while t he metabolic changes may hold true for the still viable cells and effects such as decreased plasma membrane proteins can sustain an increased BLI signal. Additionally other factors such as tumor size, shape and vasculature can influence the penetration of the photons and become important on later time points following therapy. Tumor size reduction enhances the penetration of photons which may result in an overestimation of the number of viable cells.

From this perspective, we suggest that BLI can be useful to monitor therapy but requires sequential scans to obtain the complete BLI response profile. Additionally further experiments will be necessary to elucidate the exact mechanisms of BLI flare which may hold promises and new perspectives to follow therapy induced changes. For instance, the BLI flare may be related to apoptosis which may serve as an early indication of response reflected as therapy-induced apoptosis.

Nevertheless, our results together with other reports, suggest that BLI will not beat FDG-PET as an early predictive marker for response. FDG-

PET was able to depict decreased metabolism before the tumor had reduced in size, which offers possibilities for early response assessment. Additionally FDG-PET is able to measure small metabolic changes following therapy and allows to follow-up the dynamics of therapeutic agents on the cell metabolism. In our study the FDG uptake decreased immediately in both treatment groups being related to the immediate induction of apoptosis. Nevertheless the effect of cyclophosphamide was more pronounced with more apoptosis and almost complete disappearance of the tumors as depicted in the example (**Figure 3**). On the other hand the effect of temsirolimus on tumor survival was fast (fast induction of apoptosis and fast shrinkage of tumor) while it did not result in complete disappearance of the tumor. This was not reflected in the caliper measurement while FDG-PET suggests an increased FDG uptake on day 14 following temsirolimus which indicates regrowth of the tumor (**Figure 4**).

The effect of inflammation on the FDG uptake was small in this animal model. Previous studies in the same animal model demonstrated influx of inflammatory cells between day 7 and day 9 following cyclophosphamide therapy [5, 23]. Although no increased FDG uptake was seen on these time points we observe an FDG plateau between day 4 and day 7 following cyclophosphamide while tumor size decreases gradually. Unlike cyclophoshamide, temsirolimus does not induce major influx of inflammatory cells [23]. Overall, this study adds more value to the use of FDG-PET for pre-clinical assessment of molecular response allowing to evaluate the effectiveness and function of novel anti-cancer therapies.

Conclusion

In this study we demonstrate an early significant BLI flare following two types of therapeutics. This was most likely related to metabolic changes, transient changes in transcription or altered blood protein concentrations induced by the therapy, but did not necessarily reflect viability. As a result BLI did not correlate to the FDG-PET, tumor size response and apoptosis response.

Acknowledgment

Address correspondence to: Dr. Mottaghy FM, Klinik für Nuklearmedizin, Universitätsklinikum der RWTH Aachen, Pauwelsstraße 30, 52074 Aachen, GERMANY Tel: +49-241-8088740; E-mail: fmottaghy@ukaachen.de

References

[1] Quon A and Gambhir SS. FDG-PET and beyond: molecular breast cancer imaging. J Clin Oncol 2005; 23: 1664-1673.

[2] Spaepen K, Stroobants S, Dupont P, Vandenberghe P, Maertens J, Bormans G, Thomas J, Balzarini J, De Wolf-Peeters C, Mortelmans L and Verhoef G. Prognostic value of pretransplantation positron emission tomography using fluorine 18-fluorodeoxyglucose in patients with aggressive lymphoma treated with high-dose chemotherapy and stem cell transplantation. Blood 2003; 102: 53-59.

[3] Schwimmer J, Essner R, Patel A, Jahan SA, Shepherd JE, Park K, Phelps ME, Czernin J and Gambhir SS. A review of the literature for whole-body FDG PET in the management of patients with melanoma. Q J Nucl Med 2000; 44: 153-167.

[4] Morris MJ, Akhurst T, Larson SM, Ditullio M, Chu E, Siedlecki K, Verbel D, Heller G, Kelly WK, Slovin S, Schwartz L and Scher HI. Fluorodeoxyglucose positron emission tomography as an outcome measure for castrate metastatic prostate cancer treated with antimicrotubule chemotherapy. Clin Cancer Res 2005; 11: 3210-3216.

[5] Brepoels L, Stroobants S, Vandenberghe P, Spaepen K, Dupont P, Nuyts J, Bormans G, Mortelmans L, Verhoef G and De Wolf-Peeters C. Effect of corticosteroids on 18F-FDG uptake in tumor lesions after chemotherapy. J Nucl Med 2007; 48: 390-397.

[6] Kubota R, Yamada S, Kubota K, Ishiwata K, Tamahashi N and Ido T. Intratumoral distribution of fluorine-18-fluorodeoxyglucose in vivo: high accumulation in macrophages and granulation tissues studied by microautoradiography. J Nucl Med 1992; 33: 1972-1980.

[7] Lembert N. Firefly luciferase can use L-luciferin to produce light. Biochem J 1996; 317: 273-277.

[8] Lembert N and Idahl LA. Regulatory effects of ATP and luciferin on firefly luciferase activity. Biochem J 1995; 305: 929-933.

[9] Branchini BR, Magyar RA, Murtiashaw MH, Anderson SM, Helgerson LC and Zimmer M. Site-directed mutagenesis of firefly luciferase

active site amino acids: a proposed model for bioluminescence color. Biochemistry 1999; 38: 13223-13230.

[10] Inouye S and Shimomura O. The use of Renilla luciferase, Oplophorus luciferase, and apoaequorin as bioluminescent reporter protein in the presence of coelenterazine analogues as substrate. Biochem Biophys Res Commun 1997; 233: 349-353.

[11] Blasberg RG. In vivo molecular-genetic imaging: multi-modality nuclear and optical combinations. Nucl Med Biol 2003; 30: 879-888.

[12] Rehemtulla A, Stegman LD, Cardozo SJ, Gupta S, Hall DE, Contag CH and Ross BD. Rapid and quantitative assessment of cancer treatment response using in vivo bioluminescence imaging. Neoplasia 2000; 2: 491-495.

[13] Thompson JF, Hayes LS and Lloyd DB. Modulation of firefly luciferase stability and impact on studies of gene regulation. Gene 1991; 103: 171-177.

[14] Svensson RU, Barnes JM, Rokhlin OW, Cohen MB and Henry MD. Chemotherapeutic agents up-regulate the cytomegalovirus promoter: implications for bioluminescence imaging of tumor response to therapy. Cancer Res 2007; 67: 10445-10454.

[15] Keyaerts M, Heneweer C, Gainkam LO, Caveliers V, Beattie BJ, Martens GA, Vanhove C, Bossuyt A, Blasberg RG and Lahoutte T. Plasma protein binding of luciferase substrates influences sensitivity and accuracy of bioluminescence imaging. Mol Imaging Biol 2011; 13: 59-66.

[16] Kim KI, Kang JH, Chung JK, Lee YJ, Jeong JM, Lee DS and Lee MC. Doxorubicin enhances the expression of transgene under control of the CMV promoter in anaplastic thyroid carcinoma cells. J Nucl Med 2007; 48: 1553-1561.

[17] Hingorani M, White CL, Zaidi S, Merron A, Peerlinck I, Gore ME, Nutting CM, Pandha HS, Melcher AA, Vile RG, Vassaux G and Harrington KJ. Radiation-mediated up-regulation of gene expression from replication-defective adenoviral vectors: implications for sodium iodide symporter gene therapy. Clin Cancer Res 2008; 14: 4915-4924.

[18] Mandl SJ, Mari C, Edinger M, Negrin RS, Tait JF, Contag CH and Blankenberg FG. Multi-modality imaging identifies key times for annexin V imaging as an early predictor of therapeutic outcome. Mol Imaging 2004; 3: 1-8.

[19] Ibrahimi A, Vande Velde G, Reumers V, Toelen J, Thiry I, Vandeputte C, Vets S, Deroose C, Bormans G, Baekelandt V, Debyser Z and Gijsbers R. Highly efficient multicistronic lentiviral vectors with peptide 2A sequences. Hum Gene Ther 2009; 20: 845-860.

[20] Deroose CM, Reumers V, Gijsbers R, Bormans G, Debyser Z, Mortelmans L and Baekelandt V. Noninvasive monitoring of long-term lentiviral vector-mediated gene expression in rodent brain with bioluminescence imaging. Mol Ther 2006; 14: 423-431.

[21] Krak NC, Boellaard R, Hoekstra OS, Twisk JW, Hoekstra CJ and Lammertsma AA. Effects of ROI definition and reconstruction method on quantitative outcome and applicability in a response monitoring trial. Eur J Nucl Med Mol Imaging 2005; 32: 294-301.

[22] Brepoels L, De Saint-Hubert M, Stroobants S, Verhoef G, Balzarini J, Mortelmans L and Mottaghy FM. Dose-response relationship in cyclophosphamide-treated B-cell lymphoma xenografts monitored with [18F]FDG PET. Eur J Nucl Med Mol Imaging 2010; 37: 1688-1695.

[23] De Saint-Hubert M, Brepoels L, Devos E, Vermaelen P, De Groot T, Tousseyn T, Mortelmans L and Mottaghy FM. Molecular imaging of therapy response with 18F-FLT and 18F-FDG following cyclophosphamide and mTOR inhibition. Am J Nucl Mol Imaging 2012; 2: 110-121.